Dalton Transactions

PAPER

View Article Online
View Journal | View Issue

Cite this: *Dalton Trans.*, 2014, **43**, 8480

Fabrication of N-doped TiO_2 coatings on nanoporous Si nanopillar arrays through biomimetic layer by layer mineralization

Yong Yan, Dong Wang* and Peter Schaaf

Received 4th December 2013,
Accepted 27th March 2014

DOI: 10.1039/c3dt53409j

www.rsc.org/dalton

Si/N-doped TiO_2 core/shell nanopillar arrays with a nanoporous structure are fabricated through a simple protein-mediated TiO_2 deposition process. The Si nanopillar arrays are used as templates and alternatively immersed in aqueous solutions of catalytic molecules (protamine, PA) and the titania precursor (titanium(IV) bis(ammonium lactato)dihydroxide, Ti-BALDH) for the layer by layer mineralization of a PA/TiO_2 coating. After a subsequent calcination, a N-doped TiO_2 layer is formed, and its thickness could be controlled by varying the cycles of deposition. Moreover, the nanoporous structure of the Si nanopillars strongly affects the formation of the TiO_2 layer. The obtained Si/TiO_2 nanocomposites show significantly improved solar absorption compared with commercially purchased TiO_2 nanoparticles.

1. Introduction

Titania (TiO_2) has attracted much attention due to its unique properties and many promising applications in environmental and energy areas ranging from photocatalysis and solar cells to lithium ion batteries.[1] However, the limited solar absorption and electrochemical activity caused by its poor electric conductivity and large bandgap is substantially lower than practically required.[2,3] For improving the electric conductivity of TiO_2, its combination with conducting agents, such as metals, metal oxides, and carbonaceous materials, has proved to be a common strategy to enhance electron transport;[4] on the other hand, fabrication of TiO_2 with a specific morphology (*e.g.* a high-aspect-ratio or nanoporous structure) is a promising pathway to modify the separation and transportation of charge carriers in TiO_2.[5] For improving the solar adsorption of TiO_2, N-doping and sensitization with low bandgap semiconductors are considered effective routes, which could improve the photocatalytic activity of TiO_2 by increasing its optical absorption coefficient and wavelength range.[6–8]

As a low bandgap semiconductor, silicon (Si, E_g = 1.12 eV) can adsorb sunlight efficiently, and furthermore, highly doped Si has excellent conductivity (ρ < 0.005 Ω cm). However, it is difficult to simply use Si in photo- or electrochemical applications due to its high valence band maximum energy and poor chemical stability in electrolytes.[9] Therefore, a composite structure, Si coated with a stable semiconductor (*e.g.* TiO_2), has been proposed to compensate these shortcomings.[10] Nevertheless, the synthesis of nanostructured TiO_2 with N-doping normally requires harsh conditions (NH_3 atmosphere, acids and bases, or organic solvents), which will degrade the material properties of Si.[6] Therefore, N-doping, morphology modification, and sensitization of TiO_2 with Si are not easy to achieve simultaneously, and investigations of synergistic effects of them are limited. Hence, devising a process for preparing N-doped TiO_2 with controlled morphology under relatively mild conditions is desirable.

Inspired by natural mineralization mechanisms, biomimetic mineralization has been recognized to offer an environmentally benign and energy efficient route for TiO_2 synthesis.[11] In this process, using peptides or its derivatives as catalytic molecules, micro- and nanostructured TiO_2 will be obtained under mild conditions.[12,13] Additionally, the morphology of the product could be controlled by the use of different templates such as $CaCO_3$ microparticles,[14] 3D diatom frustules,[15] anodized aluminum oxide templates,[16] silica spheres,[17] N-doped carbon nanotubes,[18] silk fibers,[19] peptide nanofibers,[20] graphene nanosheets,[21] and nickel foam.[22] Moreover, a recently-developed layer by layer mineralization process provides a versatile method for the formation of multilayer peptide/TiO_2 hybrid materials on templates;[14–17,21,22] and some studies have demonstrated that N-doped TiO_2 could be synthesized easily by sintering of peptide/TiO_2 composites.[20]

In this work, nanoporous Si nanopillar arrays fabricated by a combination of nanoimprint lithography and metal-assisted chemical etching are used as templates,[23] and are alternatively immersed in aqueous protamine (PA) and titanium

TU Ilmenau, Institute of Materials Engineering and Institute of Micro- and Nanotechnologies MarcoNano, Chair Materials for Electronics, Gustav-Kirchhoff-Str. 5, 98693 Ilmenau, Germany. E-mail: dong.wang@tu-ilmenau.de, peter.schaaf@tu-ilmenau.de

bis(ammonium lactato)-dihydroxide (Ti-BALDH) solution: positively charged protamine molecules are adsorbed on the Si nanopillars through a capillary effect and electrostatic attraction, and subsequently induce the hydrolysis and condensation of Ti-BALDH to form the negatively charged TiO_2, which enables layer by layer (LBL) deposition of protamine/TiO_2 hybrid materials on the surface of the Si nanopillars. After calcination, Si/N-doped TiO_2 core/shell nanopillar arrays with a nanoporous structure are obtained, which shows significantly improved solar absorption. Moreover, the thickness of the N-doped TiO_2 layer could be controlled by varying the cycles of deposition. The obtained Si/TiO_2 core/shell nanopillars might have potential applications in photocatalysis, and this study may pave the way for further controlled synthesis of Si/TiO_2 nanocomposites through biomimetic mineralization.

2. Experimental section

2.1. Fabrication of nanoporous Si nanopillar arrays

Ordered arrays of nanoporous Si nanopillars with hexagonal symmetry were fabricated from (100) oriented and highly doped p type Si wafer (B-doped, $\rho < 0.005\ \Omega$ cm) using a combination of substrate conformal imprint lithography (SCIL)[24] and metal-assisted chemical etching (MaCE).[25] A 20 nm Au film was deposited as a catalyst for the MaCE and the fabrication process is well described in our previous work.[23,26] The Au film was removed using a solution of KI and I_2 and the samples were dried with N_2 gas.

2.2. Materials and synthesis

Protamine sulfate salt from salmon (PA) was purchased from Sigma-Aldrich and used without purification. Titanium(IV) bis(ammonium lactato) dihydroxide (Ti-BALDH) aqueous solution was purchased from Alfa Aesar. 0.10 g protamine sulfate salt was added to 20 ml of pure H_2O and the catalytic molecular solution was obtained. Similarly, 0.98 g Ti-BALDH (50 wt% aqueous solution) was dissolved in 20 ml of H_2O and a transparent titania precursor solution (pH = 6.23) was prepared. The biomimetic layer by layer (LBL) titania deposition approach to prepare Si/N-doped TiO_2 core/shell nanopillar arrays is schematically illustrated in Scheme 1.

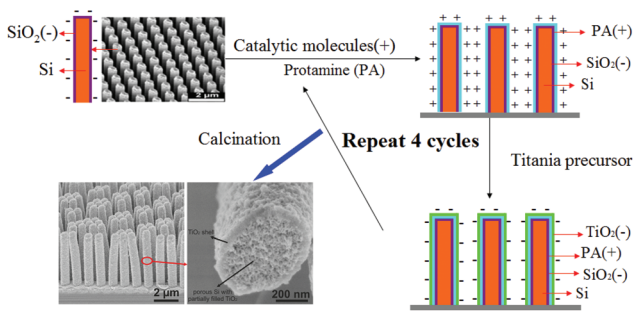

Scheme 1 Schematic illustration of the biomimetic layer-by-layer (LBL) TiO_2 mineralization on nanoporous Si nanopillar arrays.

Nanoporous Si nanopillar arrays (size: 1.0 cm × 1.0 cm) were used as templates, and firstly immersed in catalytic molecular solution (PA 5 wt‰) at room temperature for 30 min. Through capillary effects and electrostatic interactions, the positively charged PA was adsorbed on the surface of Si. After that, the Si nanopillar arrays were removed from the PA solution and rinsed with deionized water. Next, the Si nanopillar arrays with adsorbed PA were immersed in titania precursor solution at room temperature also for 30 min, and induced the hydrolysis and condensation of Ti-BALDH to form the negatively charged TiO_2 layer. After being removed from the Ti-BALDH solution and washed with deionized water, PA/TiO_2 coated Si nanopillars were obtained. By repeating the above steps for several cycles, the thickness of the PA/TiO_2 layer was stepwise increased. After calcination of these samples in Ar at 500 °C for 3 h, nitrogen atoms of the protamine were introduced into the TiO_2 structure as doped element, and Si/N-doped TiO_2 core/shell nanopillar arrays with a nanoporous structure were obtained.

2.3. Characterization

X-ray diffraction (XRD) patterns of the samples were recorded on a SIEMENS/BRUKER D5000 X-ray diffractometer using Cu-Kα radiation at 40 kV and 40 mA, with the samples being scanned from 2θ = 10°–90° at a rate of 0.02° s^{-1} in a Bragg–Brentano geometry. Scanning electron microscopy (SEM) images were taken with a Hitachi S-4800 instrument, where energy-dispersive X-ray spectrometry (EDS) was also carried out. The optical absorption in the wavelength range from UV to the visible was measured using a diffuse reflectance accessory of a UV-vis spectrometer (Cary 35 5000 UV-Vis-NIR). Zeta potentials of the samples were obtained from a Malvern Zetasizer Nano ZS. The X-ray photoelectron spectroscopy (XPS) analysis was performed using a spectrometer (Kratos Axis Ultra XPS) with monochromatized Al-Kα radiation and an energy resolution of 0.48 eV.

3. Results and discussion

The method of protamine-mediated layer by layer titania mineralization is based on previously reported studies.[14–17,21,22] Protamine (PA) is a kind of cationic protein extracted from sperm nuclei, which can induce the formation of a titania/protamine nanocomposite from a water-stable titania precursor (Ti-BALDH).[14] In the presented experiment, the nanoporous Si nanopillar arrays used as a template have a negatively charged surface due to the existence of Si–O-bearing layer (~1 nm) when it was exposed to air for several minutes.[23] This template is alternatively immersed in aqueous solutions of catalytic molecules (PA) and the titania precursor (Ti-BALDH) for the layer-by-layer fabrication of PA/TiO_2 coating (Scheme 1).

The polycationic PA molecules bind to the negatively charged Si surface and induce the formation of a TiO_2 layer from the Ti-BALDH precursor. This ability of PA to bind to the Si as well as to the TiO_2 surface enabled the layer-by-layer

(LBL) fabrication of PA/TiO_2 nanocomposite coating on the Si nanopillars. Zeta potential analysis was used to characterize the surface charge of Si nanopillars at every step during the first four cycles of this LBL TiO_2 deposition process; an oscillation for zeta potential measurement after each alternative deposition of the PA and TiO_2 was observed (Fig. 1), which is consistent with the presence of positively charged PA molecules or of negatively charged TiO_2, respectively.

In order to remove the adsorbed water, to pyrolyze the organic molecules, and to crystallize the TiO_2, the PA/TiO_2 coated Si nanopillars are calcinated at 500 °C in Ar for 3 h. Fig. 2 shows the XRD patterns of PA/TiO_2 coated Si nanopillars before and after calcination. The original TiO_2 on Si nanopillars displays an amorphous structure, and no peaks are observed between 20° and 60°, while it shows four peaks at 2θ = 25.3°, 33.1°, 37.8°, and 48.1° after calcination, which demonstrates the formation of the anatase phase. The calculated average crystallite size (using the Scherrer formula) of TiO_2 in the (101) direction is 6 nm.

Fig. 3a and b show an overview SEM image of the fabricated nanoporous Si nanopillars. The distance between two adjacent pillars (periodicity) is 1.0 μm, and the pillar height is about

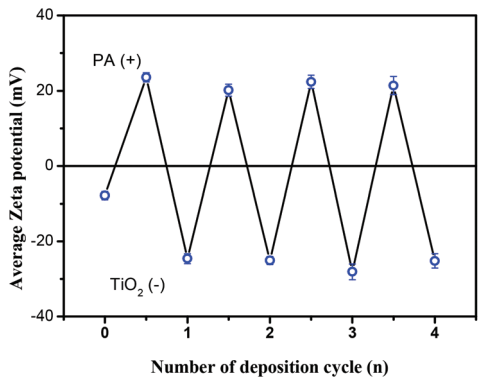

Fig. 1 Zeta-potential measurements of nanoporous Si nanopillars after each deposition step. The first measurement (layer 0) is the surface potential of the starting nanoporous Si nanopillar templates. (PA (+): protamine molecules with positive charge; TiO_2 (–):TiO_2 induced by protamine with negative charge.)

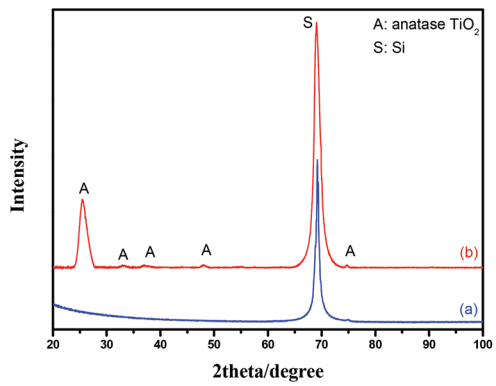

Fig. 2 XRD patterns of the PA/TiO_2 coated Si nanopillars *via* exposure to 4 LBL deposition cycles before (a) and after calcination (b).

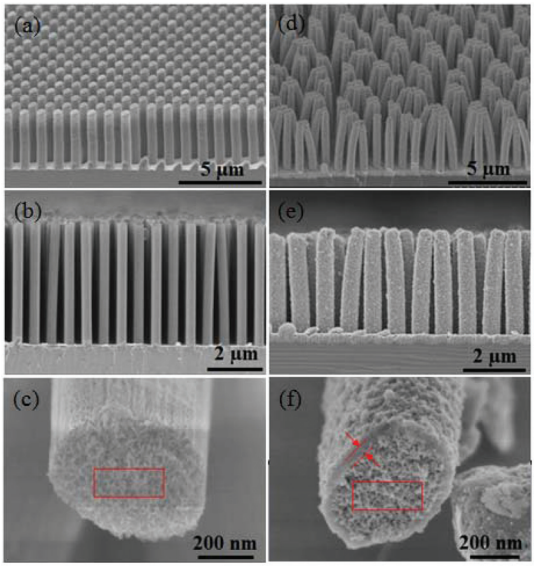

Fig. 3 SEM images of the fabricated Si nanopillars template and the TiO_2 coated Si nanopillars *via* exposure to 4 LBL deposition cycles after calcination: (a) overview of Si nanopillars; (b) side wall of Si nanopillars; (c) cross-section of Si nanopillars; (d) overview of TiO_2 coated Si nanopillars; (e) side wall of TiO_2 coated Si nanopillars; (f) cross-section of TiO_2 coated Si nanopillars.

5.2 μm; moreover, the pillars are elliptical with major and minor diameters of 613 nm and 385 nm, respectively. Fig. 3c shows the magnified images of the cross-section of the pillars, which demonstrated the existence of a three dimensional porous structure, and its pore size is about 10 nm. Fig. 3d–f show the TiO_2 coated Si nanopillars *via* exposure to 4 deposition cycles after calcination. A uniform TiO_2 coating with a thickness of 45 nm–55 nm was observed on the surface of the Si pillars, which were comprised of numerous tiny nanoparticles (<10 nm). In addition, the pore size in the bulk of Si pillars was obviously decreased, due to the filling of TiO_2 (Fig. 3f). Interestingly, more TiO_2 was filled close to the surface rather than in the center of the nanoporous pillars. An explanation for this might be that the initial deposition of TiO_2 at the surface hindered the further diffusion of PA and Ti-BALDH into the center of the pillars, leading to the lower deposition amount in the center. EDS element mapping of the TiO_2 coated Si nanopillars exhibits the presence of Ti, O, Si, N, and C species (Fig. 4). The existence of N and C species is derived from the organic pyrolysis during calcination. The XPS N 1s spectrum of this sample showed two nitrogen features: the peak with a higher binding energy centered at 401.4 eV can be assigned to nitrogen in the form of a Ti–N–O linkage,[27] and the peak with a lower binding energy located at 397.4 eV can be attributed to the nitrogen atom replacing the oxygen atoms in the TiO_2 crystal lattice with the formation of an N–Ti–N bond (Fig. 5).[28] These results demonstrate that nitrogen atoms of the protamine are introduced into the TiO_2 structure as the doped element, and the decomposition of its molecular chains forms small amounts of amorphous carbon in the TiO_2.[20] It should be noted that the distribution of Ti is

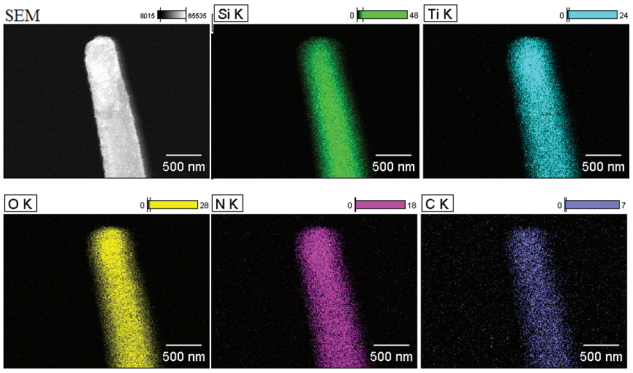

Fig. 4 EDS element mapping images of the TiO_2 coated Si nanopillars *via* exposure to 4 LBL deposition cycles after calcination (as shown in Fig. 3).

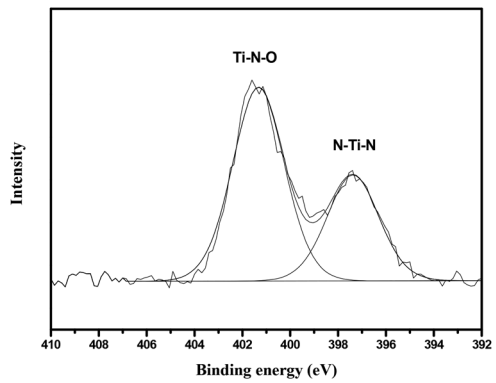

Fig. 5 N 1s XPS spectra of the TiO_2 coated Si nanopillars *via* exposure to 4 LBL deposition cycles after calcination.

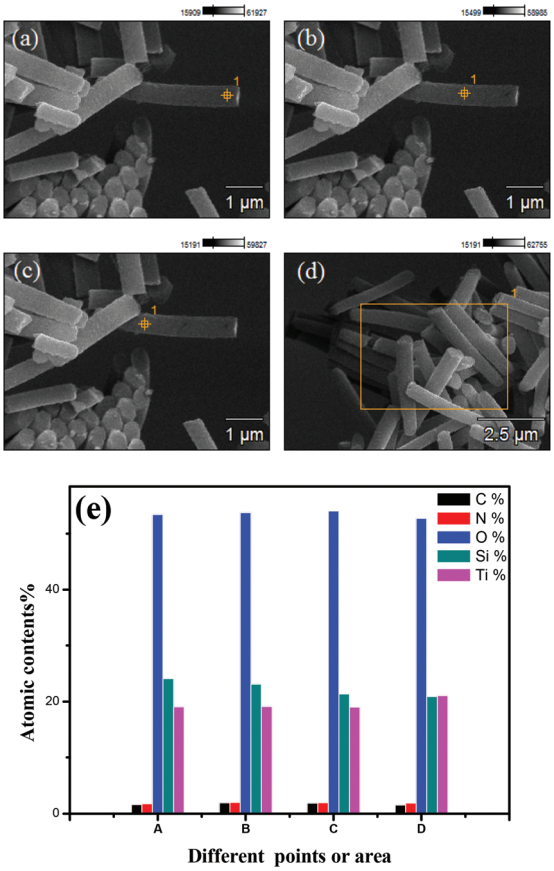

Fig. 6 EDS analysis of TiO_2 coated Si nanopillars *via* exposure to 4 LBL deposition cycles after calcination: (a–c) SEM images of the positions of the EDS measurements in points A, B, and C; (d) EDS spectrum for area D; (e) atomic contents of the sample from different points or area analysis.

wider than that of Si, indicating the structure of the Si core and TiO_2 shell. Fig. 6 exhibits the EDS spectrum of this sample, and a quantitative calculation demonstrates that the atomic ratio of Ti/Si is close to 1 for both points and area analysis, indicating that the TiO_2 deposition through biomimetic LBL mineralization is uniform. However, the content of Ti slightly increases from position A to C (from bottom to top) for TiO_2 coated Si nanopillars. This result might be induced by the lower concentration of PA and Ti-BALDH in the bottom of the Si pillars, because the PA and Ti-BALDH molecules will be partially consumed by the adsorption or reaction in the diffusion process from the top to the bottom.

To allow a deeper understanding of the formation of the TiO_2 coating, Si nanopillars coated with different cycles of deposition after calcination are characterized. After 1 cycle of deposition, a TiO_2 shell with a thickness of 10–15 nm is formed, and the porous structure on the surface of the nanopillars still remains. The filling of the porous pillar interiors is limited as the pore size in the cross-section is similar as initially (Fig. 7a and d). After 4 cycles of deposition, the thickness of the TiO_2 shell is increased to 45–55 nm, and the porous structure on the surface of the nanopillars was almost fully covered by TiO_2 layers. Moreover, TiO_2 also clearly exists in the center of the nanopillars with decreasing pore size in the cross-section (Fig. 7b and e). The thickness of the TiO_2 shell is further increased to 70–80 nm after 8 cycles of deposition, and the surface of the nanopillars becomes very rough with the appearance of numerous TiO_2 nanoparticles; in addition, the interior of the pillars seems to be completely filled with TiO_2 (Fig. 7c and f).

Compared with other reports, it is observed that biomimetic LBL TiO_2 deposition on nanoporous Si nanopillars is more efficient than that of other templates.[22–26] The ability of the catalytic molecules to bind to both the templates and the TiO_2 through electrostatic attraction is considered the key factor for this process. The experimental results indicate that the porous structure of the used Si nanopillars also strongly affects the formation of the TiO_2 layer. For comparison, solid Si nanopillars (no pores)[23] are used in an identical TiO_2 deposition process. The thickness of the formed TiO_2 shell is only 10–15 nm after 4 cycles, which is much thinner than that of nanoporous Si nanopillars (Fig. 8). One explanation might be that the nanoporous structure can enhance the adsorption of PA and Ti-BALDH through the much higher surface area and capillary effects, which induce more TiO_2 formation in both the surface and the interiors of the Si nanopillars.

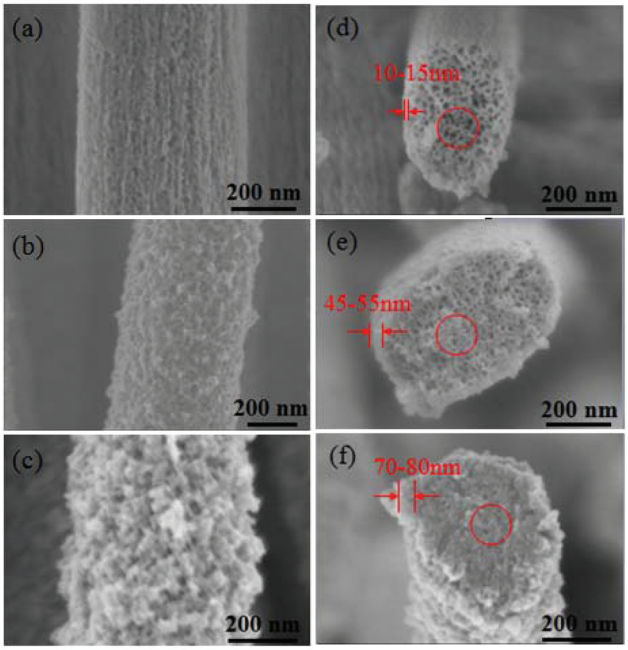

Fig. 7 SEM images of TiO_2 coated Si nanopillars *via* exposure to different LBL deposition cycles after calcination: side wall of Si nanopillars with (a) 1 cycle of deposition; (b) 4 cycles of deposition; (c) 8 cycles of deposition; cross-section of Si nanopillars with (d) 1 cycle of deposition; (e) 4 cycles of deposition; (f) 8 cycles of deposition.

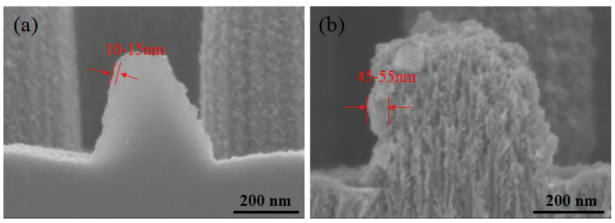

Fig. 8 SEM images of TiO_2 coating on solid (a) and nanoporous (b) Si nanopillars *via* exposure to 4 LBL deposition cycles after calcination: (a) cross-section in the bottom of TiO_2 coated solid Si nanopillars; (b) cross-section in the bottom of TiO_2 coated nanoporous Si nanopillars.

Fig. 9 shows the UV-vis absorption spectra of purchased TiO_2 nanoparticles (Degussa P25) in comparison with the presented TiO_2 coated Si nanopillars (4 LBL deposition cycles after calcination). P25 shows a steep increase in absorption at wavelengths of 400 nm due to the intrinsic bandgap of crystalline anatase TiO_2. Compared with P25, the TiO_2 coated Si nanopillars show a significantly enhanced absorption in the region of visible light, which can be attributed to the synergistic effect between N doping and Si sensitization.

4. Conclusions

In summary, Si/N-doped TiO_2 core/shell nanopillar arrays with a nanoporous structure are produced through a protamine-mediated layer-by-layer TiO_2 mineralization. The thickness of the N-doped TiO_2 layer can be controlled by varying the cycles of deposition, and the experimental results demonstrate that the nanoporous structure of the Si nanopillars strongly affects and enhances the formation of the TiO_2 layer. The obtained Si/TiO_2 nanocomposites show significantly improved solar adsorption. As a consequence, the obtained Si/TiO_2 core/shell nanopillars might have potential applications in photocatalysis. This study may pave the way for further controlled synthesis of Si/TiO_2 nanocomposites through biomimetic mineralization.

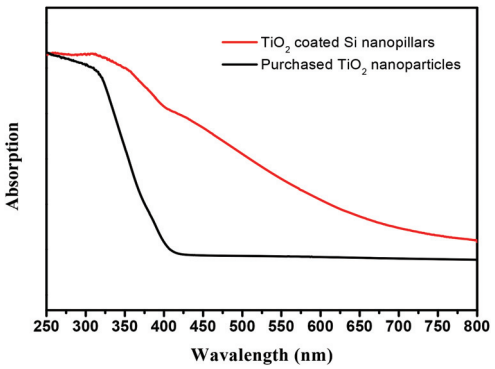

Fig. 9 UV-vis absorption spectra of purchased TiO_2 nanoparticles (Degussa P25) and TiO_2 coated Si nanopillars *via* exposure to 4 LBL deposition cycles after calcination.

Acknowledgements

The authors are grateful to Dr Ran Ji from SUSS MicroTec Lithography GmbH (Munich) for performing the substrate conformal imprint lithography (SCIL). They also acknowledge Mrs Manuela Breiter, Mrs Birgitt Hartmann, Mrs Ilona Marquardt, and Mr Joachim Döll from TU Ilmenau for their help with sample preparation, and Mrs Magali Camargo for her help in zeta-potential measurements. This work was partially supported by a grant (NanoBatt TNA VII-1/2012) from the state of Thuringia (TMWAT by LEG Thüringen) and co-financed by the European Union within the frame of the European Funds for Regional Development (EFRD). Yong Yan is supported by means of a doctoral scholarship from the Carl Zeiss Stiftung (Germany).

Notes and references

1 X. B. Chen and S. S. Mao, *Chem. Rev.*, 2007, **107**, 2891.
2 Y. Yan, B. Hao, D. Wang, G. Chen, E. Markweg, A. Albrecht and P. Schaaf, *J. Mater. Chem. A*, 2013, **1**, 14507.
3 X. Lu, G. Wang, T. Zhai, M. Yu, J. Gan, Y. Tong and Y. Li, *Nano Lett.*, 2012, **12**, 1690.
4 X. Xin, X. F. Zhou, J. H. Wu, X. Y. Yao and Z. P. Liu, *ACS Nano*, 2012, **6**, 11035.
5 Z. Zheng, B. Huang, J. Lu, Z. Wang, X. Qin, X. Zhang, Y. Dai and M. H. Whangbo, *Chem. Commun.*, 2012, **48**, 5733.

6 R. Asahi, T. Morikawa, T. Ohwaki, K. Aoki and Y. Taga, *Science*, 2001, **293**, 269.
7 Y. L. Lee, C. F. Chi and S. Y. Liau, *Chem. Mater.*, 2010, **22**, 922.
8 J. Hensel, G. M. Wang, Y. Li and J. Z. Zhang, *Nano Lett.*, 2010, **10**, 478.
9 Y. J. Hwang, A. Boukai and P. D. Yang, *Nano Lett.*, 2009, **9**, 410.
10 Y. W. Chen, J. D. Prange, S. Dühnen, Y. Park, M. Gunji, C. E. Chidsey and P. C. McIntyre, *Nat. Mater.*, 2011, **10**, 539.
11 J. L. Sumerel, W. Yang, D. Kisailus, J. C. Weaver, J. H. Choi and D. E. Morse, *Chem. Mater.*, 2003, **15**, 4804.
12 G. P. Smith, K. J. Baustian, C. J. Ackerson and D. L. Feldheim, *J. Mater. Chem.*, 2009, **19**, 8299.
13 S. L. Sewell and D. W. Wright, *Chem. Mater.*, 2006, **18**, 3108.
14 Y. J. Jiang, D. Yang, L. Zhang, Q. Y. Sun, X. H. Sun, J. Li and Z. Y. Jiang, *Adv. Funct. Mater.*, 2009, **19**, 150.
15 Y. N. Fang, Q. Z. Wu, M. B. Dickerson, Y. Cai, S. Shian, J. D. Berrigan, N. Poulsen, N. Kroger and K. H. Sandhage, *Chem. Mater.*, 2009, **21**, 5704.
16 J. D. Berrigan, T. S. Kang, Y. Cai, J. R. Deneault, M. F. Durstock and K. H. Sandhage, *Adv. Funct. Mater.*, 2011, **21**, 1693.
17 N. R. Haase, S. Shian, K. H. Sandhage and N. Kroger, *Adv. Funct. Mater.*, 2011, **21**, 4243.
18 W. J. Lee, J. M. Lee, S. T. Kochuveedu, T. H. Han, H. Y. Jeong, M. Park, J. M. Yun, J. Kwon, K. No, D. H. Kim and S. O. Kim, *ACS Nano*, 2012, **6**, 935.
19 M. B. Dickerson, C. L. Knight, M. K. Gupta, H. R. Luckarift, L. F. Drummy, M. L. Jespersen, G. R. Johnson and R. R. Naik, *Mater. Sci. Eng., C*, 2011, **31**, 1748.
20 T. Nonoyama, T. Kinoshita, M. Higuchi, K. Nagata, M. Tanaka, K. Sato and K. Kato, *J. Am. Chem. Soc.*, 2012, **134**, 8841.
21 B. Hao, Y. Yan, X. B. Wang and G. Chen, *ACS Appl. Mater. Interfaces*, 2013, **5**, 6285.
22 X. B. Wang, Y. Yan, B. Hao and G. Chen, *ACS Appl. Mater. Interfaces*, 2013, **5**, 3631.
23 D. Wang, R. Ji, S. Du, A. Albrecht and P. Schaaf, *Nanoscale Res. Lett.*, 2013, **8**, 42.
24 R. Ji, M. Hornung, M. A. Verschuuren, R. van de Laar, J. van Eekelen, U. Plachetka, M. Moeller and C. Moormann, *Microelectron. Eng.*, 2010, **87**, 963.
25 X. Li and P. W. Bohn, *Appl. Phys. Lett.*, 2000, **77**, 2572.
26 D. Wang, S. Schönherr, R. Ji, A. Herz, C. Ronning and P. Schaaf, *J. Micromech. Microeng.*, 2013, **23**, 074004.
27 J. Wang, W. Zhu, Y. Zhang and S. Liu, *J. Phys. Chem. C*, 2007, **111**, 1010.
28 G. Yang, Z. Jiang, H. Shi, T. Xiao and Z. Yan, *J. Mater. Chem.*, 2010, **20**, 5301.